CHAPTER 5

Mathematical description of polarisation dispersion in fibres with linear and circular birefringence

In this Chapter a theoretical model for describing the fibre birefringence and the PSPs of the fibre in the presence of twist, is presented. The theoretical model is developed through three stages which are:

(a) Deriving a matrix description for a fibre with twist (assuming no intrinsic linear birefringence) with external stress.
(b) Analogous to the solution in (a), a matrix description for fibre with twist and intrinsic linear birefringence is derived.
(c) From (b), the matrix description for the PSPs will be obtained, and a compact vector equation describing the DGD as a function of twist, is derived.

It will be shown that random mode coupling can be easily introduced into the model. At the end of the chapter, a numerical model giving the DGD as a function of externally applied twist in spun fibres with sinusoidal spin will be introduced. The theoretical descriptions of birefringence and DGD will be useful in later chapters, where experimental work is presented:

In *Chapter 6* an analysis and prediction of the DGD and birefringence in different kinds of fibres as a function of twist, is presented. This is applicable to cabled fibres where a small amount of twist is often unavoidable during fibre fabrication, cabling and deployment.

In *Chapter 7* the theory is extended to include the forward-backward propagation with reflection (ideal scattering), in order to describe and analyse POTDR data in the presence of twist.

The structure of this chapter is as follows. Section 5.1 first describes the combination of birefringence effects in optical fibres by using the local birefringence vector. Then the matrix solution for fibres with uniform linear and twist induced circular birefringence will be derived. Section 5.2 defines the PEMs and PSPs from an arbitrary rotation matrix. From the PSP matrix the DGD equation is obtained for the twisted fibre, subsequently the PSP for an ensemble of fibre pieces will be derived, which allows the introduction of mode coupling into the twisted fibre. Section 5.3 discusses the vector solution for the DGD in the rotating reference frame obtained from the matrix solution in Section 5.2. It will be shown that the DGD of twisted fibre increases linearly with length, neglecting some small oscillatory terms. The ideal elastic twist to give the minimum DGD, for different values of internal linear birefringence, will be obtained, and the reduction in DGD for uniformly twisted spun fibre will be shown. Section 5.4 outlines a numerical simulation for the SOP evolution of the only recently commercially available spun fibre with sinusoidal spin. The main objective of this section is to introduce the relevant parameters for the sinusoidally twisted spun fibre, in order to understand and calculate by numerical integration, the DGD reduction in this kind of fibre. The results of the simulation and measurements will be shown and discussed in Chapter 6.

5.1 Mueller matrix description of the SOP evolution in twisted fibres

5.1.1 Combining the co-existing birefringent effects in optical fibres

In a single mode fibre we can assume negligible dichroism (no PDL), uniform polarisation over the spatial mode field [55], and preservation of polarisation orthogonality at all points along the fibre [42]. The magnitude of the Stokes vector is constrained to unity, and using the Poincaré sphere representation, the polarisation properties of a single mode fibre can be expressed by a real 3×3 rotation matrix $\mathbf{R}(l, \omega)$. This is equivalent to the Jones matrix given in Equation 2.7 in Chapter 2 as

$$\vec{\mathbf{s}}(l,\omega) = \mathbf{R}(l,\omega)\vec{\mathbf{s}}(0,\omega) \tag{5.1}$$

where $\vec{\mathbf{s}}(l,\omega)$ is the Stokes vector at length l in the fibre at the optical source frequency ω. In practice $\mathbf{R}(l, \omega)$ in single mode fibres is a complicated function of both position and frequency (Chapter 3). For short lengths of fibres with uniform linear and/or circular birefringence, the SOP evolution along a fibre, at a single frequency, can be visualised by a geometrical interpretation of the local birefringence vectors on the Poincaré sphere [37].

A single finite rotation from one SOP on the Poincaré sphere to another, e.g. from SOP_{in} in Figure 5.1(a) to SOP_B, can be completely specified by the direction and location of the axis of rotation $\delta\hat{\beta}$, with the rotation angle turned through $\delta\beta = \left\|\delta\vec{\beta}\right\|$. For the case of uniform linear $\delta\vec{\beta}_L$, or circular birefringence $\delta\vec{\beta}_C$, as treated in Chapter 3, the rotation or birefringence vector is fixed in the equatorial plane on the Poincaré sphere for $\delta\vec{\beta}_L$ and along the poles for $\delta\vec{\beta}_C$ [28]. The SOP evolution which describes just a simple circle around the linear and circular birefringence vectors is shown in Figure 5.1(a) and (b) respectively; the direction of the rotation vectors is defined in the fixed laboratory frame and coincides with the PEM of the fibre.

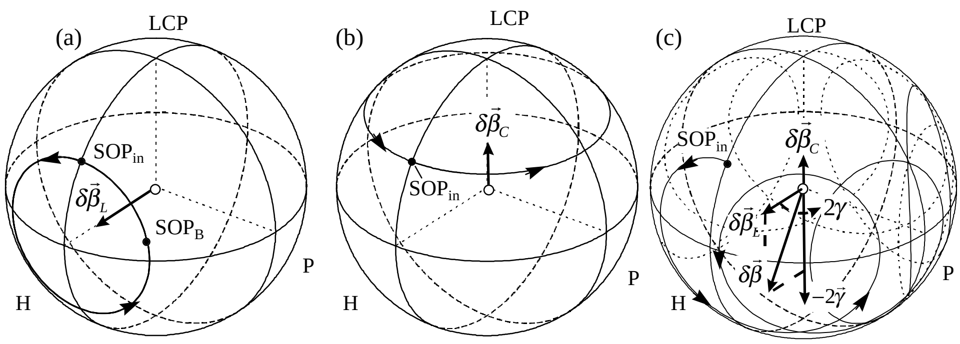

Figure 5.1 Birefringence vectors and evolution of polarisation for (a) linear birefringence, (b) circular birefringence and (c) intrinsic linear and circular birefringence with $\gamma/\delta\beta_L = 0.05$.

If birefringence effects co-exist e.g. (i) linear birefringence due to shape birefringence and externally applied pressure, or, (ii) twist induced circular birefringence and external stress, the resultant birefringence vector is simply the vectorial sum of the individual birefringence vectors on the Poincaré sphere. However, for internal linear birefringence due to shape birefringence (Section 3.3), and twist as indicated in Figure 5.2, the co-existing linear and circular birefringence vectors cannot be added vectorially on the Poincaré sphere, because there is also a geometrical rotation of the linear birefringence axes at twice the twist rate, on the Poincaré sphere, as indicated in Figure 5.1(c). However by considering an infinitesimal rotation (on local basis), the rotations commute and vector addition can be used, because the order of rotation is irrelevant. These infinitesimal rotations can be expressed as a rotation around the resultant local birefringence vector $\delta\vec{\beta}$, by the following differential vector equation [37], [126]

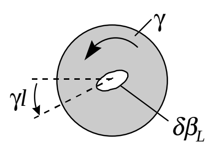

Figure 5.2 Fibre with internal birefringence $\delta\beta_L$, twisted at rate γ.

$$\frac{d\vec{\mathbf{s}}(l,\omega)}{dl} = \delta\vec{\beta}(l,\omega)\times\vec{\mathbf{s}}(l,\omega) \tag{5.2}$$

Equation (5.2) describes the SOP evolution along the fibre at a fixed source frequency. A similar vector equation describing the polarisation dispersion by the so-called polarisation dispersion vector, $\vec{\Omega}$, has been introduced in Section 3.4 and will be important in this chapter [37], [126]

$$\frac{d\vec{\mathbf{s}}(l,\omega)}{d\omega} = \vec{\Omega}(l,\omega)\times\vec{\mathbf{s}}(l,\omega) \tag{5.3}$$

Equation (5.3) describes the first order dependence of the SOP with respect to the optical frequency (see Chapter 3). By combining the two vector Equations (5.2) and (5.3) the general Equation 3.40 in Section 3.4 describing the evolution of the PSP with length and frequency, can be found.

5.1.2 Mathematical formulation for describing fibres with linear and twist induced circular birefringence

In this subsection an analytical solution of the SOP evolution in fibres exhibiting uniform linear and circular birefringence will be derived by solving Equation (5.2). From this solution the polarisation dispersion in a fibre with twist will be obtained by using Equation (5.3).

By assuming an infinitesimal fibre section with uniform linear and circular birefringence the two rotations commute as mentioned above, and can be described by a single rotation vector. The birefringence vector in Equation (5.2) can be now described as a vector sum of a rotating linear birefringence vector along the equator of the sphere, with twice the twist rate γ, and a fixed circular birefringence vector which aligned along the poles of the sphere. The local birefringence vector can be expressed on the Poincaré sphere as (see Figure 5.1(c))

$$\delta\vec{\beta}(l) = \begin{pmatrix} \delta\beta_x(l) \\ \delta\beta_y(l) \\ \delta\beta_z \end{pmatrix} = \begin{pmatrix} \delta\beta_L \cos(2\gamma l + 2\alpha_o) \\ \delta\beta_L \sin(2\gamma l + 2\alpha_o) \\ \delta\beta_C \end{pmatrix} \tag{5.4}$$

where α_0 is the angle of the local fast fibre axis orientation at $l = 0$ ($-\pi < 2\alpha_0 \leq \pi$). The wavelength dependence in Equation (5.4) has been temporarily dropped because only the solution at a single frequency is of interest. The twist rate has been defined as positive for right-handed twist, which induces L-rotary optical activity[1], such that the plane of polarisation rotates counter clockwise when looking towards the source. The vector Equation (5.2) can be re-written in matrix form using the local birefringence vector in Equation (5.4) as

$$\frac{d\vec{\mathbf{s}}(l)}{dl} = \mathbf{A}(l)\vec{\mathbf{s}}(l) \qquad \textit{where} \qquad \mathbf{A}(l) = \begin{pmatrix} 0 & -\delta\beta_z & \delta\beta_y(l) \\ \delta\beta_z & 0 & -\delta\beta_x(l) \\ -\delta\beta_y(l) & \delta\beta_x(l) & 0 \end{pmatrix} \tag{5.5}$$

The matrix **A**(*l*) is a skew Hermitian matrix (anti symmetric matrix) and its transpose is equal to the matrix multiplied by minus one $\mathbf{A}^T(l) = -\mathbf{A}(l)$. Equation (5.5) consists of three coupled differential equations $ds_{1,2,3}/dl$, which cannot be solved directly, because of the length dependence of the eigenvectors in the matrix. In the next subsection, a solution for **A**(*l*) will be derived assuming $\delta\beta_x$ and $\delta\beta_y$ are independent of *l* (**A** = constant), as in the case of a twisted fibre with no internal birefringence, but external applied stress. This solution will then help by analogy, to derive the solution for fibre with twist and internal birefringence by applying the rotating reference frame.

5.1.2.1 Solution for the constant skew symmetric matrix $\mathbf{A}(\delta\vec{\beta})$.

The solution for the linear-homogenous differential Equation (5.5) with a constant matrix $\mathbf{A}(\delta\vec{\beta})$ to give the desired rotation matrix **R**, which analogous to the scalar case, is an exponential function

$$\vec{\mathbf{s}}(l) = e^{\mathbf{A}(\delta\vec{\beta})l}\vec{\mathbf{s}}(0) = \mathbf{R}(\delta\vec{\beta}, l)\vec{\mathbf{s}}(0) \tag{5.6}$$

The validity of the exponential form can be proved by expanding the matrix exponential $e^{\mathbf{A}l}$ into a Taylor series, substituting the expansion into the left hand side of Equation (5.5), and differentiating with respect to *l*

---

[1] If there is only birefringence due to twist, right-hand twist can be described by a left circular retarder (LCR). On the Poincaré sphere, the circular birefringence vector is then pointing with its fast axis in the direction of the left circular polarisation pole (LCP), Figure 5.1(b), which is defined as positive and where, after convention, a LCR retards RCP with respect to LCP.

$$\frac{d\vec{\mathbf{s}}(l)}{dl} = \left(0 + \frac{\mathbf{A}}{1!} + \frac{2\mathbf{A}^2}{2!}l + \frac{3\mathbf{A}^3}{3!}l^2 + \ldots\right)\vec{\mathbf{s}}(0)$$

$$= \mathbf{A}\left(\mathbf{I} + \frac{\mathbf{A}}{1!}l + \frac{\mathbf{A}^2}{2!}l^2 + \frac{\mathbf{A}^3}{3!}l^3 + \ldots\right)\vec{\mathbf{s}}(0)$$

$$= \mathbf{A}e^{\mathbf{A}l}\vec{\mathbf{s}}(0) \tag{5.7}$$

where **I** is the 3×3 unit matrix (identity matrix). Equation (5.7) proves that this solution is correct and further shows that for a skew symmetric matrix the exponential $e^{\mathbf{A}l}$ is a rotation matrix. Next, the rotation matrix **R** which is in exponential form, will be decomposed into a proper 3×3 matrix, where it will be helpful to normalise the components of the matrix $\mathbf{A}(\vec{\beta})$ to $\delta\beta = \sqrt{\delta\beta_x^2 + \delta\beta_y^2 + \delta\beta_z^2}$, which is the angular rotation speed[2] of $\delta\vec{\beta}$ **,** such that

$$\mathbf{B}(\delta\hat{\beta}) = \mathbf{A}(\delta\vec{\beta}) / \delta\beta \quad or \quad \mathbf{B}_{ij} = \sum_{k=1}^{3} \varepsilon_{ijk}\delta\hat{\beta}_k \tag{5.8}$$

where $\delta\hat{\beta} = \delta\vec{\beta}/\delta\beta$ is the unit vector pointing in the direction of rotation, and ε_{ijk} is the permutation symbol, which is defined as

$$\varepsilon_{ijk} = \begin{cases} 1 & if\ i,j,k\ is\ a\ cyclic\ permutation\ of\ 1,2,3 \\ -1 & if\ i,j,k\ is\ a\ non-cyclic\ permutation\ of\ 1,2,3 \\ 0 & otherwise \end{cases} \tag{5.9}$$

The skew-symmetric matrix **B** in the normalised form has some useful properties which include

$$\mathbf{B}^{2n+1} = (-1)^n \mathbf{B} \quad and \quad \mathbf{B}^{2n+2} = (-1)^n \mathbf{B}^2 \qquad n = 0,1,2,\ldots \tag{5.10}$$

---

[2] $\delta\beta$ is the imaginary value of the complex eigenvalues from the skew-symmetric matrix $k(\lambda)$ = $\det(\mathbf{I}\lambda - \mathbf{A}) = \lambda^3 + \delta\beta\lambda = 0$ with eigenvalues $\lambda_1 = 0$ and $\lambda_{2,3} = \pm j\delta\beta$

Equation (5.10) can be proven by using the property that $\delta\hat{\beta}_x^2 + \delta\hat{\beta}_y^2 + \delta\hat{\beta}_z^2 = 1$. Re-writing the exponential solution $e^{\mathbf{A}l}$ given in Equation (5.6) in terms of the normalised matrix **B** multiplied by the angular rotation speed as determined in Equation (5.8), the exponential matrix solution is now

$$\mathbf{R}\left(\delta\vec{\beta}\, l\right) = e^{\mathbf{B}\delta\beta l} \tag{5.11}$$

Expanding (5.11) into a Taylor series and using the properties of the normalised skew-symmetric matrices given in Equation (5.10) it is possible to obtain

$$\begin{aligned} e^{\mathbf{B}\delta\beta\cdot l} &= \left(\mathbf{I} + \frac{\mathbf{B}}{1!}\delta\beta\, l + \frac{\mathbf{B}^2}{2!}\left(\delta\beta\, l\right)^2 + \frac{\mathbf{B}^3}{3!}\left(\delta\beta\, l\right)^3 + \ldots\right) \\ &= \mathbf{I} + \mathbf{B}\sum_{n=0}^{\infty}\frac{(-1)^n\left(\delta\beta\, l\right)^{2n+1}}{(2n+1)!} + \mathbf{B}^2 - \mathbf{B}^2\sum_{n=0}^{\infty}\frac{(-1)^n\left(\delta\beta\, l\right)^{2n}}{(2n)!} \\ &= \mathbf{I} + \mathbf{B}\sin\left(\delta\beta\, l\right) + \mathbf{B}^2\left(1 - \cos\left(\delta\beta\, l\right)\right) \\ &= \mathbf{R}\left(\delta\vec{\beta}\, l\right) \end{aligned} \tag{5.12}$$

In Equation (5.12) the Taylor series of the sine and cosine have been used to obtain the rotation matrix **R**, which describes the SOP rotation around an fixed elliptical birefringence vector $\delta\vec{\beta}$ on the Poincaré sphere as shown in Figure 5.3(a)

$$\vec{\mathbf{s}}(l) = \mathbf{R}(\delta\vec{\beta}\, l)\vec{\mathbf{s}}(0) \tag{5.13}$$

Since the rotation matrix in Equation (5.13) is a unity orthogonal matrix, the determinant det(**R**) = 1, and its inverse equals its transpose ($\mathbf{R}^{-1} = \mathbf{R}^{T}$), whilst the rotation in the opposite direction is given by

$$\mathbf{R}\left(-\delta\vec{\beta}\, l\right) = \mathbf{R}^{T}\left(\delta\vec{\beta}\, l\right) = \mathbf{R}^{-1}\left(\delta\vec{\beta}\, l\right) \tag{5.14}$$

Equation (5.13) can be also written in a vector form by using the reverse of the arguments used in Equations (5.2) to (5.5), and using $\delta\hat{\beta}\cdot\delta\hat{\beta}^{T} = \mathbf{I} + \mathbf{B}^2$,

$$\vec{\mathbf{s}}(l) = \cos\left(\delta\beta\, l\right)\vec{\mathbf{s}}(0) + \sin\left(\delta\beta\, l\right)\left(\delta\hat{\beta} \times \vec{\mathbf{s}}(0)\right) + \left(1 - \cos\left(\delta\beta\, l\right)\right)\left(\delta\hat{\beta}\,\vec{\mathbf{s}}(0)\right)\delta\hat{\beta} \qquad (5.15)$$

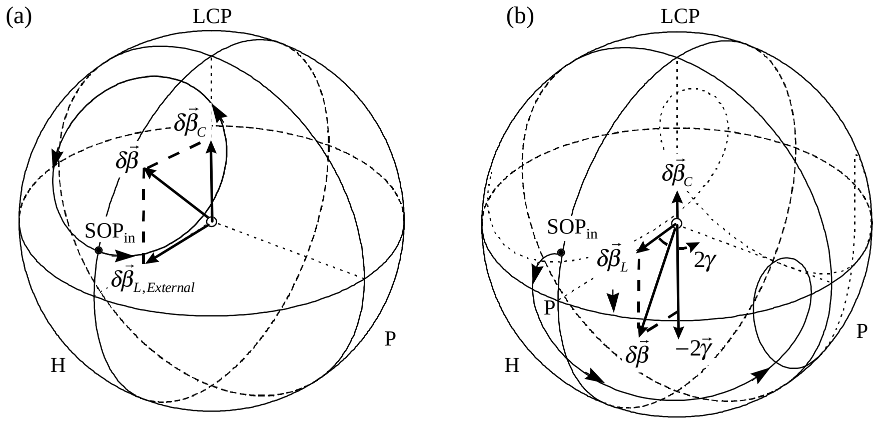

Figure 5.3 Birefringence vectors and evolution of polarisation for (a) external linear and circular birefringence (intrinsic $\delta\beta_L$ = 0), and (b) intrinsic linear birefringence and circular birefringence with $\gamma/\delta\beta_L$ = 0.1.

5.1.2.2 The rotating sphere

The three coupled differential equations $\mathrm{d}s_{1,2,3}/\mathrm{d}l$ given in the matrix Equation (5.5) cannot be solved directly, as shown for the constant matrix **A** in Subsection 5.1.2.1, because of the length dependence of the eigenvectors in the matrix. By rotating the Poincaré sphere at twice the twist rate, relative to the fixed laboratory frame, a constant elliptical eigenvector can be found in the rotating frame [37], as indicated in Figure 5.3(b).

The rotation of the Poincaré sphere around its fundamental axes *x*-*y* and *z* can be derived by writing the components of the skew symmetric matrix $\mathbf{B}\delta\beta\bullet l$ in its fundamental transformation basis, by using the appropriate rotation generators $\hat{\mathbf{r}}_x, \hat{\mathbf{r}}_y, \hat{\mathbf{r}}_z$, which determine the rotation axes as

$$\mathbf{B}\delta\beta\, l = \left(\hat{\mathbf{r}}_x\delta\hat{\beta}_x + \hat{\mathbf{r}}_y\delta\hat{\beta}_y + \hat{\mathbf{r}}_z\delta\hat{\beta}_z\right)\delta\beta\, l \qquad (5.16)$$

where $$\hat{\mathbf{r}}_x = \begin{bmatrix} 0 & 0 & 0 \\ 0 & 0 & -1 \\ 0 & 1 & 0 \end{bmatrix}, \quad \hat{\mathbf{r}}_y = \begin{bmatrix} 0 & 0 & 1 \\ 0 & 0 & 0 \\ -1 & 0 & 0 \end{bmatrix}, \quad \hat{\mathbf{r}}_z = \begin{bmatrix} 0 & -1 & 0 \\ 1 & 0 & 0 \\ 0 & 0 & 0 \end{bmatrix}.$$

As specified in Figure 5.1 the twist birefringence vector is along the poles of the sphere $\delta\hat{\beta} = \begin{bmatrix} 0 & 0 & 1 \end{bmatrix}^T$, and the rotation generator $\hat{\mathbf{r}}_z$ is used to generate the rotation around the poles (rotating frame), with twice the twist rate, in order to transform Equation (5.5) into a constant matrix. The rotation of the sphere with twice the twist around the z-axis can be written in exponential form by using Equation (5.11) and Equation (5.16) as

$$\mathbf{R}_z(\alpha_\gamma) = e^{(\hat{\mathbf{r}}_z \alpha_\gamma)} \quad and \quad \mathbf{R}_z(-\alpha_\gamma) = e^{-(\hat{\mathbf{r}}_z \alpha_\gamma)} \tag{5.17}$$

where $\alpha_\gamma = 2\gamma l + 2\alpha_o$. The proper matrix form of Equation (5.17) is obtained by using the same transformation as for the general rotation matrix given in Equation (5.12)

$$\mathbf{R}_z(\alpha_\gamma) = \begin{pmatrix} \cos(\alpha_\gamma) & -\sin(\alpha_\gamma) & 0 \\ \sin(\alpha_\gamma) & \cos(\alpha_\gamma) & 0 \\ 0 & 0 & 1 \end{pmatrix} \tag{5.18}$$

and with rotation in the opposite direction as

$$\mathbf{R}_z(-\alpha_\gamma) = \mathbf{R}_z^{-1}(\alpha_\gamma) = \mathbf{R}_z^T(\alpha_\gamma) \tag{5.19}$$

Re-writing Equation (5.5) now with either Equations (5.17) or (5.19) in order to get a constant matrix $\mathbf{A}_c$ (independent of l), gives

$$\frac{d\vec{\mathbf{s}}(l)}{dl} = \mathbf{R}_z(\alpha_\gamma)\mathbf{A}_c\mathbf{R}_z^{-1}(\alpha_\gamma) \cdot \vec{\mathbf{s}}(l) \tag{5.20}$$

where $\mathbf{R}_z(\alpha_\gamma)\mathbf{A}_c\mathbf{R}_z^{-1}(\alpha_\gamma)$ is equal to $\mathbf{A}(l)$ and $\mathbf{A}_c$ is given by

$$\mathbf{A}_c = \begin{pmatrix} 0 & -\delta\beta_C & 0 \\ \delta\beta_C & 0 & -\delta\beta_L \\ 0 & \delta\beta_L & 0 \end{pmatrix} \tag{5.21}$$

The next step is to introduce the rotating frame, where the SOP evolution $\vec{\mathbf{s}}(l)$ in the rotating frame can be expressed as

$$\vec{\mathbf{s}}_r(l) = \mathbf{R}_z^{-1}(\alpha_\gamma)\vec{\mathbf{s}}(l) \tag{5.22}$$

where the subscript *r* denotes rotating frame. Inserting Equation (5.22) into Equation (5.20) yields

$$\frac{d\vec{\mathbf{s}}_r(l)}{dl} + \mathbf{R}_z^{-1}(\alpha_\gamma)\frac{d\mathbf{R}_z(\alpha_\gamma)}{dl}\vec{\mathbf{s}}_r(l) = \mathbf{A}_c\vec{\mathbf{s}}_r(l) \tag{5.23}$$

where

$$\mathbf{R}_z^{-1}(\alpha_\gamma)\frac{d\mathbf{R}_z(\alpha_\gamma)}{dl} = \mathbf{R}_z^{-1}(\alpha_\gamma)\frac{d\alpha_\gamma}{dl}\frac{d\mathbf{R}_z(\alpha_\gamma)}{d\alpha_\gamma} = 2\gamma\hat{\mathbf{r}}_z \tag{5.24}$$

inserting Equation (5.24) into Equation (5.23) and re-arranging the equation, the proposed constant rotation matrix inside the rotating frame is obtained as

$$\frac{d\vec{\mathbf{s}}_r(l)}{dl} = \mathbf{A}_r\vec{\mathbf{s}}_r(l) = \begin{pmatrix} 0 & (2-g)\gamma & 0 \\ -(2-g)\gamma & 0 & -\beta_L \\ 0 & \beta_L & 0 \end{pmatrix}\vec{\mathbf{s}}_r(l) \tag{5.25}$$

or written in vector form

$$\frac{d\vec{\mathbf{s}}_r(l)}{dl} = \begin{pmatrix} \delta\beta_L \\ 0 \\ -(2-g)\gamma \end{pmatrix} \times \vec{\mathbf{s}}_r(l) = \delta\vec{\beta}_r \times \vec{\mathbf{s}}_r(l) \tag{5.26}$$

Normalising the elements of the skew-symmetric matrix $\mathbf{A}_r$ in Equation (5.25) in the same way, as carried out for the skew-symmetric matrix in Equation (5.8) by defining $\mathbf{A}_r\left(\delta\vec{\beta}_r\right) = \mathbf{B}_r\left(\delta\hat{\beta}_r\right)\delta\beta_r$, the differential Equation (5.25) can be re-written as

$$\frac{d\vec{\mathbf{s}}_r(l)}{dl} = \mathbf{B}_r\delta\beta_r\vec{\mathbf{s}}_r(l) \tag{5.27}$$

where $\mathbf{B}_r$ describes the normalised rotation with rotation axis determined by the unit vector $\delta\hat{\beta}_r$, and $\delta\beta_r$ is the angular rotation speed given by

$$\delta\beta_r = \sqrt{\delta\beta_L^2 + \left(g\gamma - 2\gamma\right)^2} \tag{5.28}$$

The rotation vector $\delta\vec{\beta}_r$ in the rotating reference frame, agrees with the one derived by Ulrich and co-workers [37] by geometrical means using the Poincaré sphere. The vector $\delta\vec{\beta}_r$ (without subscript) is also indicated in Figure 5.1(c) and Figure 5.3(b).

5.1.2.3 Solution for the twisted fibre with internal linear birefringence

Because the matrix $\mathbf{A}_r = \mathbf{B}_r\delta\beta_r$ is constant, the differential equation given in Equation (5.25) or (5.27), can be solved in an analogous way to the exponential solution used in Subsection 5.1.2.1. By expansion into a Taylor series, the proper rotation matrix in the rotating frame is obtained as

$$\vec{\mathbf{s}}_r(l) = \mathbf{R}\vec{\mathbf{s}}_r(0) \tag{5.29}$$

where

$$\mathbf{R}(\delta\vec{\beta}_r\, l) = \mathbf{I} + \sin(\delta\beta_r\, l)\mathbf{B}_r + \left(1 - \cos(\delta\beta_r\, l)\right)\mathbf{B}_r^2 \tag{5.30}$$

Finally transforming Equation (5.29) back into the laboratory frame using Equation (5.22) yields

$$\vec{\mathbf{s}}(l) = \mathbf{R}_z(\alpha_\gamma)\mathbf{R}(\delta\vec{\beta}_r\, l)\mathbf{R}_z^T(2\alpha_o)\vec{\mathbf{s}}(0) = \mathbf{R}_\gamma\vec{\mathbf{s}}(0) \tag{5.31}$$

Re-introducing the temporarily dropped frequency dependence of the rotation matrix, the final equation for the fibre with twist can be written as

$$\vec{\mathbf{s}}(l,\omega) = \mathbf{R}_\gamma(l,\omega)\vec{\mathbf{s}}(0,\omega) \tag{5.32}$$

where $\mathbf{R}_\gamma(l,\omega)$ is the final unitary rotation matrix for simulating a fibre with uniform linear $\delta\beta_L$, and circular birefringence $\delta\beta_C$, whose individual frequency co-efficients have been derived in Section 3.3. It should be also realised that the solution given in Equation (5.31) also covers the simpler case of fibre with twist and external stress, but no internal birefringence, as given in Equation (5.12).

5.1.2.4 Solution for an ensemble of fibre pieces with linear and circular birefringence

The matrix solution for the twisted fibre given in Equation (5.32) is for a single fibre piece. The SOP evolution along a uniformly twisted fibre can be modelled by dividing the fibre in an ensemble of short fibre pieces, as shown in Figure 5.4, and using matrix multiplication, so that the SOP at the output of the N^{th} element $\vec{\mathbf{s}}(l_N)$ is given by

$$\vec{\mathbf{s}}(l_N) = \mathbf{R}_z(\alpha_N)\mathbf{r}_N\mathbf{R}_z^T(2\alpha_o)\vec{\mathbf{s}}(0) \tag{5.33}$$

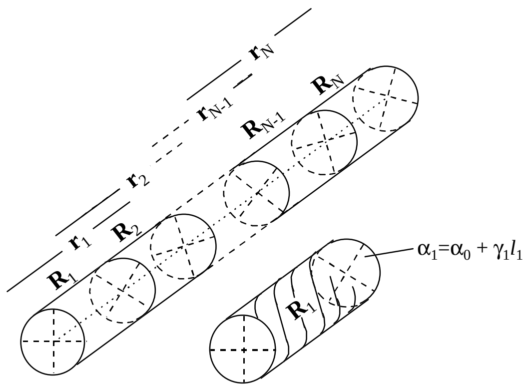

Figure 5.4 Fibre model for an ensemble of twisted fibre pieces, a random axes deviation at the interfaces of the fibres is also indicated.

where $\alpha_N = 2\alpha_o + 2\sum_{n=1}^{n=N}\gamma_n l_n$ and $\mathbf{r}_N = \mathbf{R}_N\mathbf{R}_{N-1}...\mathbf{R}_2\mathbf{R}_1 = \mathbf{R}_N\mathbf{r}_{N-1}$. By using Equation (5.33) the SOP evolution for elastically twisted fibre has been plotted in Figure 5.1(c).

For the twisted fibre from this subsection onwards, the subscript r denoting explicitly the birefringence in the rotating frame will be dropped, ($\delta\vec{\beta}_r \Rightarrow \delta\vec{\beta}$) which is written mainly for convenience, and because for uniform twisted fibre our main interest will be in the resulting birefringence in the rotating reference frame for many of the following equations. Care has to be taken not to confuse the birefringence in the rotating reference frame, with the local birefringence vector in the twisted fibre.

5.2 The derivation of the polarisation eigen modes and principal states of polarisation from the fibre rotation matrix

In Chapter 3 the terms PEMs and PSPs were used in the sense of describing the rotation of the SOP around a rotation axis for a birefringent element with respect to length using the PEMs and with respect to frequency using the PSP. In this subsection the PEMs and PSPs for an arbitrary rotation matrix will be obtained.

5.2.1 The PEMs of the fibre

The PEMs of a fibre are a typical eigenvalue problem, with input SOP equal to output SOP along the fibre. They are only properly defined for a constant fibre ‘matrix’ with fixed rotation axis as treated in Subsection 5.1.2.1. Since any rotation matrix **R** can be written in an exponential form $\mathbf{R} = e^{\mathbf{A}} = e^{\mathbf{B}\delta\beta}$, as proved in Section 5.1, the eigenvalues of **R** are determined by the eigenvalues of the skew-symmetric matrix **A.** These are obtained from $\det(\mathbf{I}\lambda - \mathbf{A}) = \lambda^3 + \delta\beta\lambda = 0$, with eigenvalue solutions $\lambda_1 = 0$ and $\lambda_{2,3} = \pm j\delta\beta$. It then follows that the eigenvalues of the rotation matrix **R** are $\lambda_1 = e^0 = 1$ and $\lambda_{2,3} = e^{\pm j\delta\beta} = \cos(\delta\beta) \pm j\sin(\delta\beta)$, where $\delta\beta$ determines the rotation angle, and the eigenvalue solution $\lambda_1 = 1$, can be used to calculate the real eigenvector (rotation axis) of the rotation matrix.

5.2.2 The PSP of the fibre

Polarisation dispersion arises as a result of the frequency dependence of the rotation matrix $\mathbf{R}(l,\omega)$. In the principal state model, polarisation mode dispersion is described by a rotation of the output SOP on the Poincaré sphere versus optical frequency, as shown in Figure 3.19, Section 3.4. The rotation axes define the two principal states of polarisation (PSPs), which are fixed to a first order approximation over a small wavelength range [126], [127]. The frequency dependence of the output SOP for a fixed input SOP is given by differentiating Equation (5.1)

$$\frac{d\vec{s}_{out}}{d\omega} = \frac{d\mathbf{R}}{d\omega}\vec{s}_{in} = \frac{d\mathbf{R}}{d\omega}\mathbf{R}^T\vec{s}_{out} = \mathbf{\Omega}\,\vec{s}_{out} \tag{5.34}$$

The polarisation dispersion matrix is defined by $\mathbf{\Omega}$ and the input SOP has been taken as fixed with frequency. Every exponential matrix with a skew-symmetric matrix as its exponent, is an orthogonal matrix [167], and Equation (5.34) can be written, in general, in exponential form as

$$\frac{d\vec{s}_{out}}{d\omega} = \frac{de^{\mathbf{A}}}{d\omega} e^{-\mathbf{A}} \vec{s}_{out} = \frac{d\mathbf{A}}{d\omega} \vec{s}_{out} = \mathbf{\Omega}\, \vec{s}_{out} = \vec{\Omega} \times \vec{s}_{out} \tag{5.35}$$

Equation (5.35) shows that the polarisation dispersion matrix $\mathbf{\Omega}$ is a skew-symmetric describing a rotation of the SOP on the Poincaré sphere with frequency, and can be re-written in vector form, to give the corresponding DGD vector $\vec{\Omega}$, as given by Equation (5.2). The rotation axis of $\mathbf{\Omega}$ can be assumed to be fixed over a small wavelength range (first order approximation), and the polarisation dispersion matrix can be written in the form as given by Equation (5.8), as an angular rotation speed $\left|\vec{\Omega}\right|$ around a fixed rotation axis

$$\mathbf{\Omega} = \left|\vec{\Omega}\right| \begin{pmatrix} 0 & -\hat{\Omega}_z & \hat{\Omega}_y \\ \hat{\Omega}_z & 0 & -\hat{\Omega}_x \\ -\hat{\Omega}_y & \hat{\Omega}_x & 0 \end{pmatrix} \tag{5.36}$$

where $\hat{\Omega} = \begin{bmatrix} \hat{\Omega}_x & \hat{\Omega}_y & \hat{\Omega}_z \end{bmatrix}^T$ is the component of the normalised rotation axis which determines the PSPs and

$$\left|\vec{\Omega}\right| = \sqrt{\Omega_x^2 + \Omega_y^2 + \Omega_z^2} = \sqrt{tr\left(\mathbf{\Omega}\mathbf{\Omega}^T\right)/2} = d\theta/d\omega = \Delta\tau \tag{5.37}$$

is the magnitude of the vector which determines the group delay difference between the two principal modes (see Figure 3.19, Section 3.4), where *tr* denotes the trace of the matrix.

5.2.3 *The PSP matrix for the twisted fibre and for an ensemble of fibre pieces*

The PSPs of a general rotation matrix are defined in Equation (5.34) and for a twisted fibre are obtained by differentiating the fibre matrix given in Equation (5.31), with respect to frequency, and multiplying it by its transpose [79], [127]

$$\mathbf{\Omega}(l,\omega) = \frac{d\mathbf{R}_\gamma}{d\omega}\mathbf{R}_\gamma^T = \mathbf{R}_z(\alpha_\gamma)\frac{d\mathbf{R}(\delta\vec{\beta}\,l)}{d\omega}\mathbf{R}^T(\delta\vec{\beta}\,l)\mathbf{R}_z^T(\alpha_\gamma) \tag{5.38}$$

To calculate the magnitude of the DGD, the PSPs which refer to a single point in a fibre can be evaluated in the rotating reference frame, because the reference frame is independent of wavelength[3]. Using Equation (5.37), and the property that the trace of an arbitrary matrix is not changed if left multiplied with a rotation matrix, and right multiplied with the inverse of the same rotation matrix (or vice versa)[4], the equality of the DGD in both rotating and fixed reference frame can be calculated

$$\begin{aligned}\left|\vec{\Omega}\right| &= \sqrt{1/2}\sqrt{tr\Big(\big(\mathbf{R}_z(\alpha_\gamma)\mathbf{R}'(\delta\vec{\beta}\,l)\mathbf{R}_\gamma^T\big)\big(\mathbf{R}_\gamma\mathbf{R}'^T(\delta\vec{\beta}\,l)\mathbf{R}_z^T(\alpha_\gamma)\big)\Big)} \\ &= \sqrt{1/2}\sqrt{tr\big(\mathbf{R}'(\delta\vec{\beta}\,l)\mathbf{R}'^T(\delta\vec{\beta}\,l)\big)}\end{aligned} \tag{5.39}$$

Equation (5.39) could also be used in a real measurement to calculate the DGD from the measured rotation matrices at two different frequencies, where the derivative of the rotation matrix is approximated by

$$\frac{d\mathbf{R}}{d\omega} \approx \lim_{\Delta\omega\to 0}\frac{\mathbf{R}(\omega+\Delta\omega)-\mathbf{R}(\omega)}{\Delta\omega} \tag{5.40}$$

5.2.3.1 PMD for an ensemble of twisted fibre pieces with random mode coupling

For an ensemble of fibre pieces with no random mode coupling, the PSPs along the fibre can be calculated from the fibre matrix along the fibre as given in Equation (5.33), with $\mathbf{R}_N$ specifying the N^{th} section, and $\mathbf{r}_{N-1}$ the first N–1 sections. The derivative of the resultant matrix, and from that, the polarisation dispersion matrix using Equation (5.38) can be calculated as

$$\begin{aligned}\mathbf{r}'_N &= \mathbf{R}'_N\mathbf{r}_{N-1} + \mathbf{R}_N\mathbf{r}'_{N-1} \\ \mathbf{\Omega} &= \mathbf{R}_z(\alpha_N)\mathbf{r}'_N\mathbf{r}'^T_N\mathbf{R}_z^T(\alpha_N)\end{aligned} \tag{5.41}$$

---

[3] The geometrical rotation is wavelength independent.

[4] $Tr(\mathbf{RMR}^{-1}) = Tr(\mathbf{M})$ where $\mathbf{M}$ is an arbitrary matrix, c.f. [167].

where $\alpha_N = 2\alpha_o + 2\sum_{n=1}^{n=N}\gamma_n l_n$. Random mode coupling as discussed in Section 3.4 can be introduced in Equation (5.41) by allowing a random orientation of the fibre axes between the fibre interfaces. For a uniform distribution of the fibre axes orientation X between ⟨$-\pi/2 \leftrightarrow \pi/2$ in radians⟩, the resultant fibre matrix given in Equation (5.33) can be re-written as

$$\begin{aligned}\mathbf{r}_N &= \mathbf{R}_N\mathbf{R}_{N-1}...\mathbf{R}_2\mathbf{R}_1 = \mathbf{R}_N\mathbf{r}_{N-1}\\ \mathbf{R}_N &= \mathbf{R}_Z\left(\gamma l + \mathrm{X}_N\right)\mathbf{R}_N\mathbf{R}_z^T\left(\mathrm{X}_N\right)\end{aligned} \tag{5.42}$$

and the polarisation dispersion matrix including random mode coupling is given by

$$\begin{aligned}\mathbf{r}'_N &= \mathbf{R}'_N\mathbf{r}_{N-1} + \mathbf{R}_N\mathbf{r}'_{N-1}\\ \mathbf{\Omega} &= \mathbf{r}'_N\mathbf{r}'^T_N\end{aligned} \tag{5.43}$$

The random axes alignment in Equation (5.42) may be also considered as a random walk along the fibre in which case the fibre twist along the fibre, from fibre section to fibre section, has to be summed along the fibre.

5.3 A vector description of the DGD evolution in a fibre with uniform twist

The first order dependence of the SOP, with respect to the optical frequency, can be described by the DGD vector $\vec{\Omega}$, given in Equation (5.34). In Equation (5.39) it has been shown in matrix form that the DGD magnitude of the twisted fibre can be calculated in the rotating reference frame. On evaluating the right hand side of Equation (5.34) for $\mathbf{R}(\delta\vec{\beta}\, l)$ as given by Equation (5.30), the corresponding polarisation dispersion vector $\vec{\Omega}$ in the rotating reference frame can be written in a compact vector form (derived in Appendix B), as [79]

$$\vec{\Omega} = \frac{d(\delta\beta)}{d\omega}\delta\hat{\beta}\, l + \left(\sin(\delta\beta\, l)\frac{d\left(\delta\hat{\beta}\right)}{d\omega} + \left(1-\cos(\delta\beta\, l)\right)\left(\delta\hat{\beta}\times\frac{d\left(\delta\hat{\beta}\right)}{d\omega}\right)\right) \tag{5.44}$$

The dispersion vector in Equation (5.44) is composed of two components, one is parallel to $\delta\hat{\beta}$ and grows linearly with length, whilst the other is orthogonal to $\delta\hat{\beta}$ (determined by the derivative $d(\delta\hat{\beta})/d\omega$ see Appendix B), is of constant magnitude with length, and follows a circular motion in the plane orthogonal to $\delta\vec{\beta}$ (Figure 5.5). In general $\vec{\Omega}$ is not aligned with $\delta\vec{\beta}$, as indicated in Figure 5.5, and the evolution of $\vec{\Omega}$ along the fibre describes a uniform helix in the rotating reference. The evolution of $\vec{\Omega}$ in Figure 5.5 has been plotted using Equation (5.44), showing the orthogonality of the vector $d(\delta\hat{\beta})/d\omega$ in Equation (5.44) to $\delta\vec{\beta}$. For fibre lengths larger than a couple of metres, or twist rates larger than a few turns per metre, the oscillatory terms (as will be shown), can be neglected, and the DGD becomes proportional to the frequency derivative of the magnitude of the birefringence vector

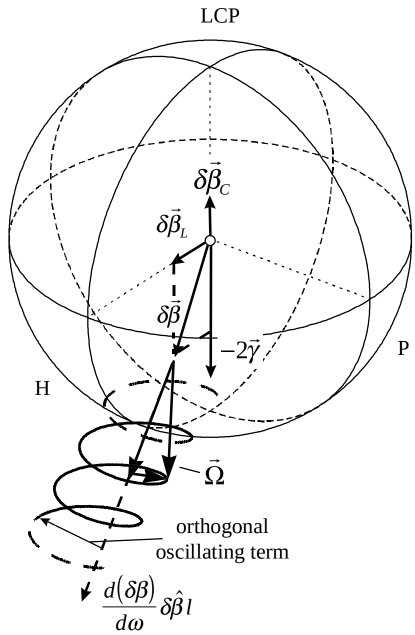

Figure 5.5 Birefringence and dispersion vector in rotating reference frame

$$\vec{\Omega} = \frac{d(\delta\beta)}{d\omega}\delta\hat{\beta}\,l = \frac{d\sqrt{\delta\beta_L^2 + (2\gamma - \delta\beta_C)^2}}{d\omega}\delta\hat{\beta}\,l = \left(\frac{\delta\beta_L\delta\beta_L' + (\delta\beta_C - 2\gamma)\delta\beta_C'}{\sqrt{\delta\beta_L^2 + (\delta\beta_C - 2\gamma)^2}}\right)\delta\hat{\beta}\,l \qquad (5.45)$$

where $\delta\beta_L' = d(\delta\beta_L)/d\omega$ and $\delta\beta_C' = d(\delta\beta_C)/d\omega$. The dispersion of the linear birefringence $\delta\beta_L'$ in a fibre may arise through a combination of stress effects and geometrical effects caused by asymmetry of the core, which are both wavelength dependent, and whose detailed dispersion magnitudes depend on the geometrical mode factor, as discussed in Section 3.3. For simplicity, because our main interest is in the DGD reduction with twist in Equation (5.45), we will at the moment assume $\delta\beta_L'$ to be independent of the geometrical mode factor ($m(\lambda)$ and $C(\lambda)$ = 1 in Equation 3.22), so that we can write

$$\delta\beta_L' \approx \frac{\delta\beta_L}{\omega} \qquad (5.46)$$

But we must also keep in mind that this can result in a 50% offset at zero twist from the actual DGD value at λ = 1.55 μm, depending on the detailed structure of the fibre (see Section 3.3). The dispersion of the twist induced circular birefringence β_C, originates in the dispersion of the stress optic coefficient *C*, such that [84]

$$\delta\beta_C' = \gamma\frac{dg}{d\omega} = \frac{g\gamma}{\omega}\frac{\omega dg}{gd\omega} = \frac{g\gamma}{\omega}\frac{\omega dC}{Cd\omega} \qquad (5.47)$$

The wavelength dependence of *C* is plotted in Figure 3.5, and its wavelength dependent term ω/g dg/dω is about 0.085 with g = 0.14 at λ = 1.55 μm for typical fibres [37], [79], [105]. Using these values for *g*, and the wavelength dependence of *C* in Equation (5.47), with some typical linear birefringence values expected in optical fibres in Equation (5.46), the magnitude of the polarisation dispersion can be calculated as a function of twist, using Equation (5.44), which includes the small fluctuation terms. In Figure 5.6 the DGD versus twist for two different fibre lengths of one and ten metres has been calculated with the above values, and using Equation (5.44).

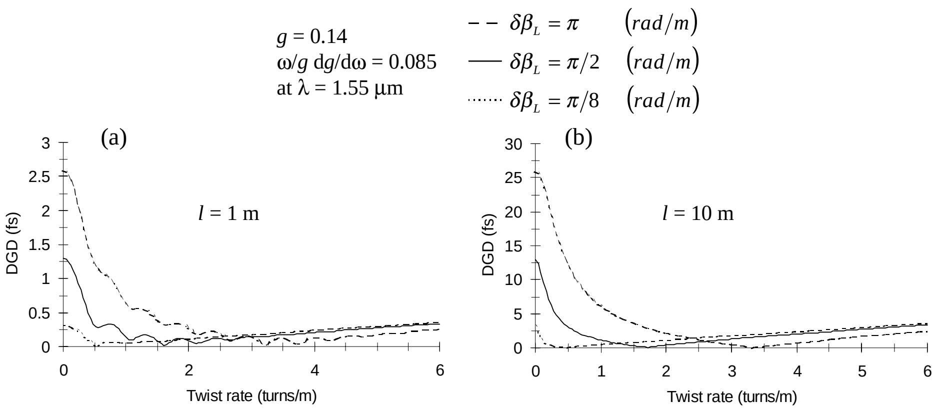

Figure 5.6 Calculated values of DGD against twist using Equation (5.44). In (a) for 1 metre fibre length where the small fluctuation terms in the DGD are visible and in (b) for 10 metre fibre length the small fluctuation terms are not visible any more.

It can be seen in Figure 5.6(a) that for the very short one metre fibre piece the small fluctuation terms are visible in the trace, whereas for the 10 metre fibre piece in (b) the linear term with length dominates in the resultant DGD. In general, the small fluctuation terms are < 1 fs, and can be neglected for fibre lengths larger than a few metres, and the DGD can be assumed to grow proportionally with the fibre length as described in Equation (5.45). Both traces in Figure 5.6 show an decrease in DGD towards zero, followed by an increase at higher twist rates, when the circular birefringence is dominant.

In Figure 5.7(a) the DGD normalised with respect to fibre length has been plotted versus twist using Equation (5.45). The ideal elastic twist rate γ_{Min} for zero DGD, where there is a change in the sign of the DGD (the fast fibre mode at that point turns into slow one and vice versa), can be obtained by setting Equation (5.45) equal to zero, and solving the equation for γ which gives the solutions

$$\gamma_{Min} = \pm \frac{\delta\beta_L}{2\pi} \sqrt{\frac{1}{2g(1-g)} \frac{Cd\omega}{\omega dC}} \approx \pm\delta\beta_L \quad (turns/m) \tag{5.48}$$

Using Equation (5.48) the ideal twist rate for fibre with different initial linear birefringence has been plotted in Figure 5.7. This value γ_{Min} could be useful in reducing the internal DGD e.g. of erbium doped fibre amplifiers which show high DGD values (Chapter 6), by applying the ideal twist rate for the corresponding DGD. In Chapter 6 the derived theory of the DGD for twisted fibres will be compared with experimental results.

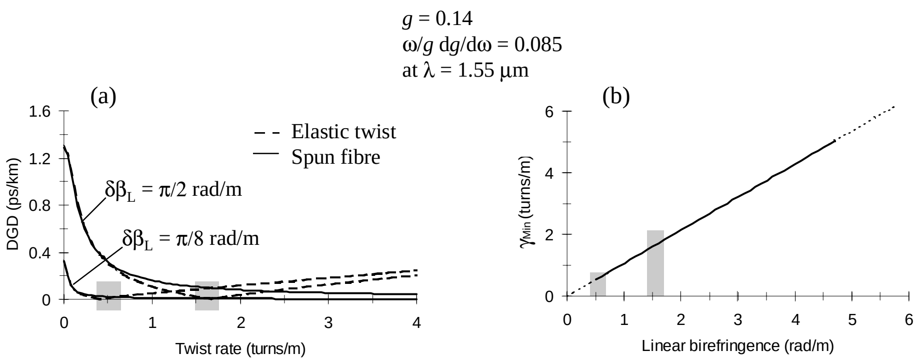

Figure 5.7 For fibre lengths larger than a few metres the small fluctuation terms in Equation (5.44) can be neglected and the DGD versus twist can be normalised to the length. In (b) the optimum twist rate for fibre with different initial linear birefringence is plotted, to obtain minimum DGD.

For spun fibres with uniform twisting during drawing, no shear stress is introduced, so that $\delta\beta_C$ is equal zero, and Equation (5.45) can be re-written as

$$\vec{\Omega} = \left(\frac{\delta\beta_L \delta\beta_L'}{\sqrt{\delta\beta_L^2 + 4\gamma^2}} \right) \delta\hat{\beta}\, l \qquad (5.49)$$

Equation (5.49) shows the reduction of the linear birefringence with the geometrical fibre axes rotation, and can be also found in that form in References like [108] or [168]. In Figure 5.8 the DGD versus twist for spun fibre assuming zero circular birefringence is plotted using Equation (5.44), which shows a continuous decrease in the DGD for increasing spin rates, with the DGD at high twist rates becoming inversely proportional to the applied spin. The small fluctuation terms in the DGD reduction can be also seen in Figure 5.8(a), for the one metre fibre piece similar to Figure 5.6(a) for the fibre with elastic twist, but now it can be also seen that for spin rates (twist rates) above a few turns per metre the oscillating term in the DGD diminishes. For fibre lengths larger than a few metres as shown in Figure 5.8(b), there is no visible fluctuation in the DGD.

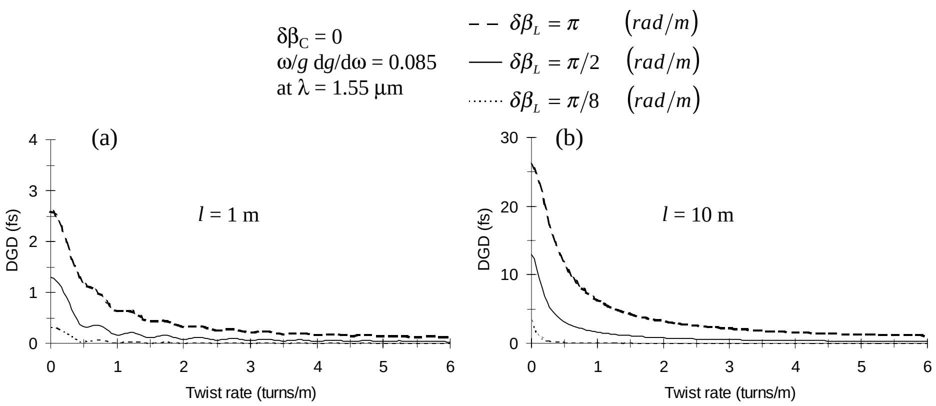

Figure 5.8 Calculated values of DGD against twist for spun fibre. In (a) for 1 metre fibre length where the small fluctuation terms in the DGD are visible and in (b) for 10 metre fibre length the small fluctuation terms are not any more visible.

The normalised DGD for spun fibre with respect to the fibre length has been plotted in Figure 5.7(a) using Equation (5.49), together with the case of elastic twist, both for initial linear birefringence of $\pi/2$ and $\pi/8$ rad/m. In comparing the ideal twist rates for elastic twisted fibres in Figure 5.7(b), which theoretically gives zero DGD, with the DGD reduction for the same twist rates and initial birefringences for spun fibre, it can be seen that the DGD of the spun fibre is reduced to about 7.5% of its initial DGD value. It seems elastic twisted fibre could have an advantage in that sense over spun fibre, although in practice it would be very difficult to achieve the necessary ideal elastic twist rate in long lengths of fibres, because the linear birefringence is usually unknown and may change along the fibre. Also spun fibre clearly has the advantage of reducing the DGD, independent of the initial fibre birefringence, continuously to zero with increasing twist. Furthermore, spun fibre is also, as mentioned in Section 3.3, quite insensitive to temperature changes [106], because no stress is generated from the twisting.

The effective retardation of the fibre can be calculated from the eigenvalues of the fibre rotation matrix given in Equation (5.32) for the twisted fibre. The eigenvalues as discussed in Subsection 5.2.1 determine the absolute rotation angle (retardation) of the rotation matrix. In Figure 5.9(a) and (b), the effective retardation of the elastically twisted fibre and spun fibre respectively, has been calculated for a one metre fibre piece. Both show the small fluctuation terms similar to the DGD in Figure 5.6(a) for elastic twist, and in Figure 5.8 for spun fibre. The effective birefringence in Figure 5.9(a) shows a decrease towards zero, but does not reach the zero birefringence because of the increase in circular birefringence which always adds to the total birefringence, followed by an increase at higher twists where the circular birefringence becomes dominant. For spun fibre in Figure 5.9(b) the effective birefringence versus twist is continuously reduced with increasing twist, because there is no circular birefringence produced.

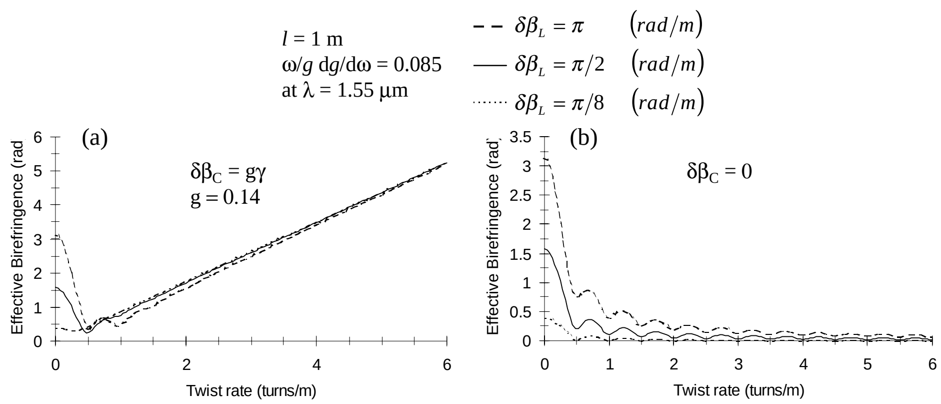

Figure 5.9 Calculated effective birefringence against twist in (a) for fibre with uniform elastic twist, and in (b) for spun fibre uniformly twisted during drawing.

5.4 Numerical calculation of the DGD reduction in spun fibre with sinusoidal spin

In this section the formalism used to simulate the SOP evolution in spun fibre with sinusoidally varying rotational frequency will be discussed including the calculation of the expected DGD in such fibres, as a function of external applied twist. In Chapter 6 the measured DGD of such spun fibres versus external applied twist will be compared to simulation results.

It is only recently that spun fibre has become available commercially (e.g. from Lycom Fibre, Denmark, owned by AT&T). These fibres are produced not by spinning the preform with constant rotational frequency while the fibre is being drawn, as was originally suggested [110], but by applying a sinusoidally varying torque to the fibre being drawn, alternatively in the clockwise and counter-clockwise directions [13], as shown in Figure 3.17. Thus the rotational frequency changes sinusoidally along the fibre, with Reference [13] claiming that the fibre contains twisted portions in excess of 4 turns/m. Further in [13] the PMD of the spun fibre is claimed to be below $0.5\, ps/\sqrt{km}$ using this method.

5.4.1 Numerical simulation of the SOP evolution in spun fibre with sinusoidal spin

For spun fibre with sinusoidal spin subject to external applied twist (as measured in Chapter 6), the local birefringence vector given in Equation (5.4) can be re-written to include the sinusoidal spin

$$\delta\vec{\beta}(l) = \begin{pmatrix} \delta\beta_L \cos(2\tilde{\alpha}_\gamma + 2\gamma l + 2\alpha_o) \\ \delta\beta_L \sin(2\tilde{\alpha}_\gamma + 2\gamma l + 2\alpha_o) \\ g\gamma \end{pmatrix} \tag{5.50}$$

with

$$\tilde{\alpha}_\gamma = A_\gamma \sin\left(2\pi\kappa_\gamma l\right) \qquad (rad) \tag{5.51}$$

where A_γ is the amplitude of the applied spin in radians and κ_γ the spatial frequency in cycles/m, which can be also expressed by the spatial period $\Lambda_\gamma = 1/\kappa_\gamma$ with units in metres. Inserting the local birefringence vector from Equation (5.50) into the differential Equation (5.5) yields

$$
\begin{aligned}
s_x' &= -\delta\beta_z s_y + \delta\beta_y s_z \\
s_y' &= \quad \delta\beta_z s_x - \delta\beta_x s_z \\
s_z' &= -\delta\beta_y s_x + \delta\beta_x s_y
\end{aligned}
\tag{5.52}
$$

Equation (5.52) consist of three first order coupled differential equation which can be solved by numerical integration. In our case a fourth order Runge-Kutta method supplied with the software package Matlab[5] has been used to solve numerically, the SOP evolution along a fibre with local eigenvectors specified in Equation (5.50), and for a fixed input SOP. In Figure 5.10(a) and (b), the SOP evolution for a fibre with an initial linear birefringence of 1.4 rad/m, but two different sinusoidal spin rates with no external twist ($\gamma = 0$), is shown. The input SOP has been chosen so that both polarisation eigenmodes of the fibre at $l = 0$ are equally excited. The SOP evolution shown in Figure 5.10(a) and (b) can be also described on the Poincaré sphere by visualising the oscillation of the linear birefringence vector, which determines the local birefringence axes, around its original unperturbed position, as indicated in the figures.

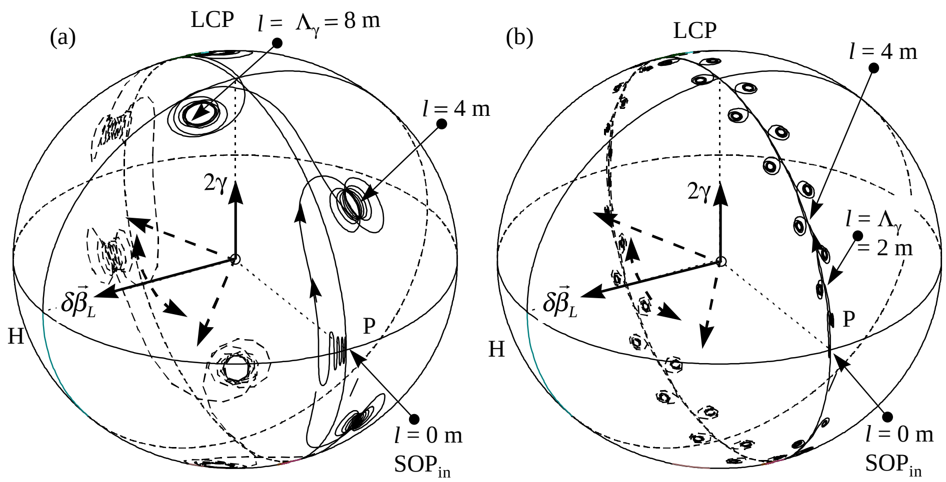

$$\tilde{\gamma}_{rms} = \frac{2\pi}{\sqrt{2}}\frac{A_\gamma}{\Lambda_\gamma} = \frac{2\pi}{\sqrt{2}}\frac{4\pi}{8} \quad (rad/m)$$
$$\delta\beta_L = 1.4 \quad (rad/m)$$

$$\tilde{\gamma}_{rms} = \frac{2\pi}{\sqrt{2}}\frac{A_\gamma}{\Lambda_\gamma} = \frac{2\pi}{\sqrt{2}}\frac{4\pi}{2} \quad (rad/m)$$
$$\delta\beta_L = 1.4 \quad (rad/m)$$

Figure 5.10 SOP evolution along spun fibre with sinusoidal spin. In (a) for $\tilde{\gamma}_{rms} \approx 1.1$ turns/m and in (b) for $\tilde{\gamma}_{rms} \approx 4.4$ turns/m.

---

[5] For the numerical simulation, the fourth order Runge-Kutta method supplied in the software package Matlab has been used. The accuracy of the numerical integration is specified in the Matlab Reference Guide, as better than 10^{-6}.

At first we can realise that the SOP on the Poincaré sphere shows some kind of periodical pattern on the sphere, determined by the chosen periodicity of $\Lambda_\gamma = 8$ metres in Figure 5.10(a) and $\Lambda_\gamma = 2$ metre in Figure 5.10(b). To understand the speed of the SOP evolution along the fibre, the speed of the local birefringence vector change along the fibre now needs to be defined next.

In Figure 5.11(a) the total rotation angle α of the fibre axis $\delta\beta_L$ is plotted versus length for uniform twist, $\alpha = 2\gamma l$, and for the fibre with sinusoidal spin with $\alpha = \tilde{\alpha}_\gamma$, see Equation (5.51), with values for the sinusoidally spun fibre, the same, as used for the simulation of the SOP in Figure 5.10(a) and (b).

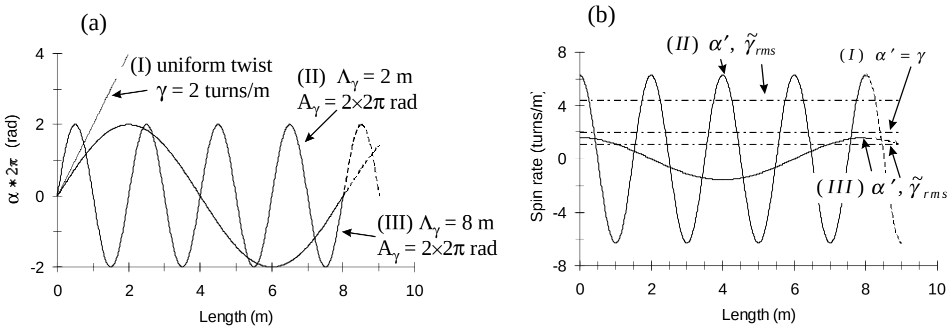

Figure 5.11 (a) the calculated total rotation angle α of the fibre axis $\delta\beta_L$, as a function of length for fibre with uniform and sinusoidal spin, and (b) the speed of the fibre axis rotation versus length.

Of more interest is the spin impressed onto the fibre which is given by the derivative of α with respect to length, $\alpha' = d\alpha/dl$. For the uniformly twisted fibre, the rotational frequency is constant and is given by the twist rate $\alpha' = \gamma$, as shown in Figure 5.11(b). For the sinusoidally applied twist the fibre axes rotational frequency is given by the derivative of Equation (5.51) as

$$\alpha' = 2\pi \frac{A_\gamma}{\Lambda_\gamma} \cos\left(2\pi\kappa_\gamma l\right) \qquad \left(rad/m\right) \tag{5.53}$$

Equation (5.53) shows clearly that for the sinusoidal twist, the applied spin (rotational frequency) changes periodically along the fibre with a spin rate amplitude determined by both the twist period and twist amplitude. In comparing later the constant spin magnitude with the sinusoidal spin the root mean square value of the sinusoidal spin is used

$$\tilde{\gamma}_{rms} = \frac{2\pi}{\sqrt{2}} \frac{A_\gamma}{\Lambda_\gamma} \qquad (rad/m) \tag{5.54}$$

In Figure 5.11(b) the spin given by Equation (5.53) is plotted for the values used for the sinusoidal fibre axis rotation in Figure 5.11(a), and the SOP evolution in Figure 5.10(a) and (b). From the spin as plotted in Figure 5.11(b) it is now also possible to understand the fast SOP changes on the Poincaré sphere in Figure 5.10(a) and (b), which coincides with the points where the local birefringence vector is in its original position and the rotational speed of the local birefringence vector is at its highest speed (at $l = n\Lambda_\gamma/2$ with n = 0, 1, 2…). At the points where the local birefringence vector changes direction the speed is the slowest and the fibre behaves almost like a simple linear retarder (just the initial linear birefringence without spin) which would show just a simple circle on the Poincaré sphere, as indicated by the overall shape of the SOP evolution in Figure 5.10(a) and (b).

5.4.2 *The DGD for spun fibre with sinusoidal spin*

The main motivation for the simulation of the SOP evolution in spun fibre is to understand how effectively this kind of spun fibre reduces the DGD for a given effective spin rate, $\tilde{\gamma}_{rms}$, in fibres with different initial linear birefringence. Next it will be explained how the DGD has been calculated from the simulated SOP data at different frequencies, and in Chapter 6, the calculated DGD for sinusoidal spun fibre will be compared with measurement results. In Chapter 6 there will also be a short discussion comparing uniformly twisted spun fibre with sinusoidally twisted spun fibre with respect to its practical possible DGD reductions (spin rate) in commercial fibre production.

For the DGD calculation we could have used Equation (5.40) by calculating the Mueller matrix at two different wavelengths around the centre wavelength at 1.55 μm. This method would need three different input SOPs times two wavelengths which would result in six simulation loops. Such a numerical simulation can be quite time-consuming even when using a fast computer[6], and for that reason it has been decided to use the arc method as discussed in

[6] The simulation results which will be shown in Chapter 6 have taken on average a couple of hours, depending on the fibre parameters and fibre length, using a Pentium 120 MHz computer to calculate the DGD.

Section 3.5 (see also Figure 3.19 in Chapter 3). This method only needs one input SOP at three different wavelengths resulting in just three simulation loops.

In the arc method, a plane is mapped through three measured SOPs at three different wavelengths with fixed input SOP. From the intersection of the plane with the sphere, the PSP direction and the rotation angle of the arc can be calculated (Figure 3.19). In real measurements as described in Section 3.5, the arc method is not ideal because noise in the system and the possibility of the output SOP lying close to the PSP degenerates the method's accuracy considerably. In simulation there is no noise but the error in the numerical calculation has to be considered which can be reduced to negligible values by choosing the correct wavelength step size so that the output SOP on the sphere shows three well separated SOPs, e.g. arc angle > 10° but < 180°. Moreover the input SOP in the simulation can be chosen so that the output SOP is well separated from the PSP (see .e.g. Figure 5.10). In Chapter 6, the DGD calculated with the numerical method for uniform elastically twisted fibre will be compared with the DGD calculated from the analytical solution given in Equation (5.45), showing perfect agreement between the two methods.